Journal of Catalysis **189,** 421–430 (2000)
doi:10.1006/jcat.1999.2720, available online at http://www.idealibrary.com on IDEAL®

Structure and Properties of Zirconia-Supported Molybdenum Oxide Catalysts for Oxidative Dehydrogenation of Propane

Kaidong Chen, Shuibo Xie, Enrique Iglesia,[1] and Alexis T. Bell[1]

Chemical and Materials Sciences Divisions, Lawrence Berkeley National Laboratory, and Department of Chemical Engineering, University of California, Berkeley, California 94720-1462

Received June 29, 1999; revised October 6, 1999; accepted October 8, 1999

Oxidative dehydrogenation (ODH) of propane was studied on zirconia-supported molybdenum oxide catalysts. The structure of the ZrO_2 support and of the dispersed MoO_x species was characterized by X-ray diffraction and by Raman and UV–visible spectroscopies. The structure of dispersed molybdena depends on the Mo surface density and on the temperature at which catalyst precursors are treated in air. Polymolybdate domains were detected by Raman at Mo surface densities below 5 Mo/nm^2. At higher surface densities, MoO_3 and $ZrMo_2O_8$ are present; their relative concentrations depend on the pretreatment temperature. Below 773 K, MoO_3 is the predominant structure at high surface densities, but $ZrMo_2O_8$ forms above 773 K. UV–visible edge energies decrease with increasing surface density for samples containing polymolybdate species, suggesting that MoO_x domains become larger as the Mo surface density increases. ODH turnover rates decrease with increasing Mo surface density on samples containing polymolybdate species and MoO_3. This trend is accompanied by an increase in the initial propene selectivity and in the vibrational frequency of Mo=O bonds. Higher Mo=O vibrational frequencies reflect stronger Mo=O bonds, which show lower ODH reactivity; therefore, the lower ODH reaction rates (per Mo atom) at higher Mo surface densities arise from the lower reactivity of Mo=O bonds, while higher initial propene selectivities arise either from the decrease of exposed Mo–O–Zr bonds or the lower reactivity of Mo=O bonds as the size of MoO_x domains increases with increasing Mo surface density. At similar Mo surface densities, samples containing predominantly $ZrMo_2O_8/ZrO_2$ show higher turnover rates and lower initial propene selectivities than those containing MoO_3 species because the vibrational frequency of the Mo=O bond for $ZrMo_2O_8/ZrO_2$ is lower than that for MoO_3. ODH turnover rates over $ZrMo_2O_8/ZrO_2$ also decreased with increasing Mo surface density, ultimately due to the increase of the particle size which leads to lower propane accessibility.

INTRODUCTION

Oxidative dehydrogenation (ODH) of light alkanes has been widely studied as a route to the corresponding alkenes. This process is thermodynamically favored at low temperatures and the presence of O_2 inhibits the carbon deposition prevalent in nonoxidative routes. Many studies have addressed the structure of ODH catalysts (1–5). The most active and selective catalysts for propane ODH are based on supported vanadia (3). Mo oxides-based catalysts have also been examined for ODH (6–10), but less thoroughly than VO_x-based catalysts, because of their lower activity. On the other hand, catalysts such as Mo–Mg–O have shown high propene selectivity in propane ODH (7).

ZrO_2 is an excellent support for ODH catalysts because it can be prepared with high surface area (>300 m^2/g), and it is structurally stable and catalytically inactive (11, 12). Strong interactions between the surface of zirconium oxyhydroxide precursors and dispersed metal oxides such as VO_x, MoO_x, and WO_x lead to stable dispersed oxides, even in the presence of water at high temperatures (13, 14). The structure of ZrO_2-supported VO_x species and their role in propane ODH have been discussed recently (14–16), but structure–function relations for dispersed MoO_x species remain less clear. Structural studies of dispersed MoO_x species show that a metastable monolayer consisting of polymolybdate species can be formed by treatment in air at around 773 K for surface densities lower than 5 Mo/nm^2 (17–20). At higher Mo surface densities, bulk MoO_3 and $ZrMo_2O_8$ form and their relative abundance depends on the temperature of the air treatment (19).

This study examines the effects of Mo surface density and catalyst treatment temperature on the structure of MoO_x–ZrO_2 catalysts and relates the structure of dispersed molybdate species to their catalytic activity and selectivity for the ODH of propane. The structures of a wide range of MoO_x–ZrO_2 samples were determined by a combination of textural characterization and spectroscopic methods. The surface areas of the catalysts were determined by the BET method. X-ray diffraction (XRD), Raman spectroscopy, and UV–visible spectroscopy were used to probe the structure and electronic properties of dispersed MoO_x species. The catalytic properties of MoO_x–ZrO_2 for propane ODH were determined using a flow reactor equipped with on-line

[1] To whom correspondence should be addressed. E-mail: bell@cchem.berkeley.edu; iglesia@cchem.berkeley.edu.

0021-9517/00 $35.00

gas chromatographic analysis. Rate constants for primary and secondary reaction pathways were obtained by kinetic analysis of steady-state catalytic data and they were used to compare catalysts on the basis of intrinsic kinetic parameters.

EXPERIMENTAL

Zirconium oxyhydroxide ($ZrO(OH)_2$) was prepared by precipitation from a zirconyl chloride solution (98%, Aldrich, Inc.) at a pH of 10 maintained constant by controlling the rate of addition of a solution of ammonium hydroxide (29.8%, Fischer Scientific, Inc.). After precipitation, the solids were washed with mildly basic ammonium hydroxide solution (pH of approximately 8) until the effluent showed no chloride ions by a silver nitrate test. The resulting solids were dried in air overnight at 393 K.

Zirconia-supported molybdena catalysts were prepared by incipient wetness impregnation of the precipitated zirconium oxyhydroxide with a solution of ammonium dimolybdate (ADM) (99%, Aldrich, Inc.) or ammonium heptamolybdate (AHM) (99%, Aldrich, Inc.). The pH of the impregnation solution was adjusted by adding nitric acid or ammonium hydroxide. The Mo^{6+} concentration in the impregnating solution was varied to change the Mo content in the final samples. After impregnation, samples were dried overnight in air at 393 K and treated in dry air (Airgas, zero grade) at 723, 773, or 873 K for 3 h. Unless otherwise noted, all samples were prepared by using ADM as the precursor, without pH modification by HNO_3 or NH_4OH.

Surface areas were measured by N_2 physisorption using a Quantasorb surface area analyzer (Quantachrome Corp.) and standard multipoint BET analysis methods. Samples were degassed for 3 h at 383 K before N_2 (Airgas, 99.999%) physisorption measurements. Powder XRD patterns were obtained at room temperature using a Siemens diffractometer and Cu $K\alpha$ radiation. A small amount of catalyst was mixed with Vaseline and spread out smoothly on a thin glass plate holder.

Raman spectra were recorded using a HoloLab series 5000 research Raman spectrometer (Kaiser Optical) equipped with a Nd:YAG laser that is frequency-doubled to 532 nm. Samples (~50 mg) were pressed into wafers at 350 MPa pressure (0.9-cm diameter; 0.1-cm thickness) and placed within a quartz cell (15). The laser was operated at a power level of 75 mW. All Raman spectra were recorded at ambient conditions.

Diffuse reflectance UV–vis spectra were recorded using a Varian-Cary 4 spectrophotometer equipped with a Harrick diffuse-reflectance attachment. MgO was used as a reference. Reflectance measurements were converted to absorption spectra using the Kubelka-Munk function. UV–vis spectra were measured in the range of 1.5–6.0 eV at ambient conditions.

Selectivity and rate measurements were carried out in a packed-bed tubular quartz reactor using 0.03- to 0.3-g catalyst samples at 703 K. Quartz powder was used as a diluent with MoO_x–ZrO_2 catalysts to prevent temperature gradients within the catalyst bed. The reactants were propane (Airgas, 99.9%) and oxygen (Airgas, 99.999%) at 14.03 and 1.74 kPa, respectively, and He (Airgas, 99.999%) was used as a diluent. On-line analysis of reactants and products was performed using a Hewlett–Packard 6890 gas chromatograph. Detailed analysis procedures were reported previously (14, 15).

C_3H_8 and O_2 conversions were varied by changing the rectant flow rate between 50 and 200 cm^3/min. Typical propane conversions were less than 2% and oxygen conversions were kept below 20%. Reaction rates and selectivities were extrapolated to zero residence time to determine the rates and the rate constants for primary ODH and combustion reactions. The effect of bed residence time on product yields was used to calculate rates and rate constants for secondary propene combustion reactions, as reported elsewhere (14–16).

RESULTS

Surface areas and Mo surface densities were measured for all MoO_x–ZrO_2 samples after treatment in air at various temperatures and the results are shown in Figs. 1 and 2. At each treatment temperature, surface areas increased with increasing MoO_3 loading up to 20 wt%, and then decreased at higher loadings (Fig. 1). Surface areas decreased with increasing air treatment temperatures for all MoO_3 loadings.

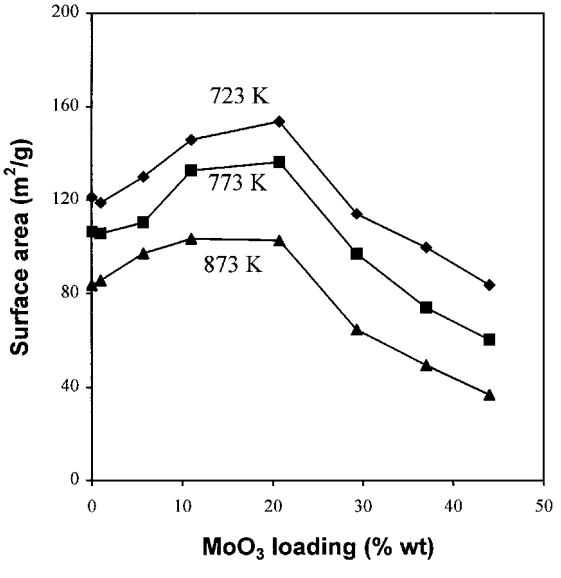

FIG. 1. BET surface areas of MoO_x–ZrO_2 catalysts treated in air at various temperatures.

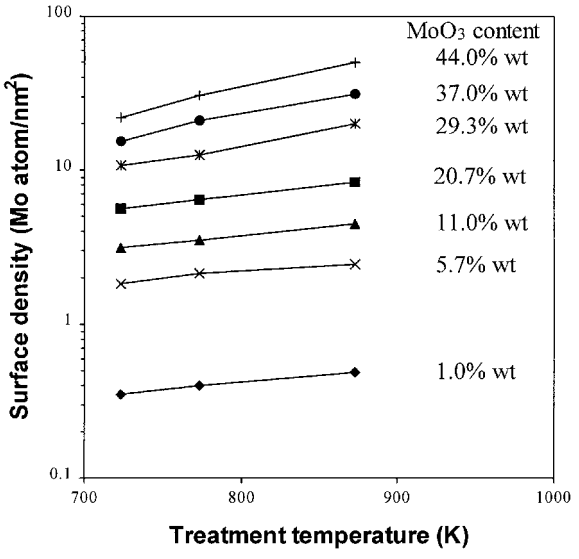

FIG. 2. Mo surface densities for MoO_x–ZrO_2 catalysts with different MoO_3 concentrations treated in air at different temperatures.

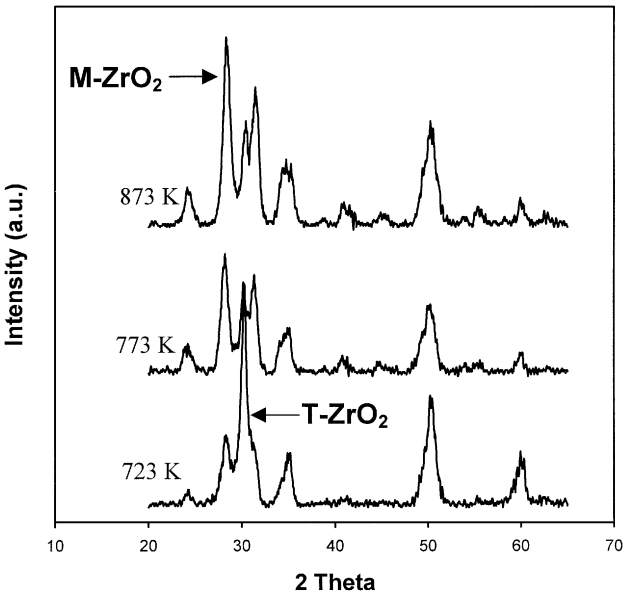

FIG. 3. XRD patterns of pure ZrO_2 calcined at different temperatures.

The Mo surface density is expressed as the number of Mo atoms per nanometer square of surface area (Mo atoms/nm^2). It was obtained by the equation

$$\text{Mo surface density} = \frac{\text{MoO}_3 \text{ percentage} \times 6.02 \times 10^{23}}{\text{Surface area} \times 144 \times 10^{18}},$$

where the unit of the surface area is m^2/g. The effects of MoO_3 loading and treatment temperature on the apparent Mo surface density are shown in Fig. 2. At each MoO_3 loading, the Mo surface density increased with the calcination temperature because of the concomitant decrease in the ZrO_2 surface area. Changing the initial pH of the impregnation solution from 2 to 10 had no effect on either the BET surface area or the Mo surface density for samples containing 1 wt% MoO_3.

The crystal structure of MoO_x–ZrO_2 samples was probed by XRD (Figs. 3–6). Tetragonal and monoclinic phases of zirconia were detected in pure ZrO_2 samples treated in air above 723 K. The intensity of the monoclinic peaks increased relative to that of peaks corresponding to tetragonal ZrO_2 with increasing treatment temperatures (Fig. 3). The addition of small amounts of MoO_3 to ZrO_2 led to significantly higher tetragonal content at all treatment temperatures (Fig. 4). In MoO_x–ZrO_2 samples with low MoO_3 concentration (11 wt% MoO_3), only tetragonal ZrO_2 was observed and crystalline MoO_x phases were not detected by XRD (Fig. 5). At high MoO_3 loadings (37 wt% MoO_3), XRD patterns for MoO_x–ZrO_2 depended strongly on the temperature of the air treatment (Fig. 6). Low temperature (723 K) led to the formation of crystalline MoO_3, while high temperature (873 K) led to the formation of a $ZrMo_2O_8$ phase. For the sample treated at 773 K, both crystalline MoO_3 and $ZrMo_2O_8$ were formed.

The Raman spectra of several MoO_x–ZrO_2 samples are shown in Figs. 7–9. All samples with Mo surface densities lower than 5 Mo/nm^2 showed similar Raman spectra (Fig. 7). A band at about 829 cm^{-1}, corresponding to Mo–O–Mo vibrations (19, 21), and a band at 920–980 cm^{-1}, assigned to Mo=O vibrations (19, 21–23) in two-dimensional polymolybdates, were detected in these samples. As

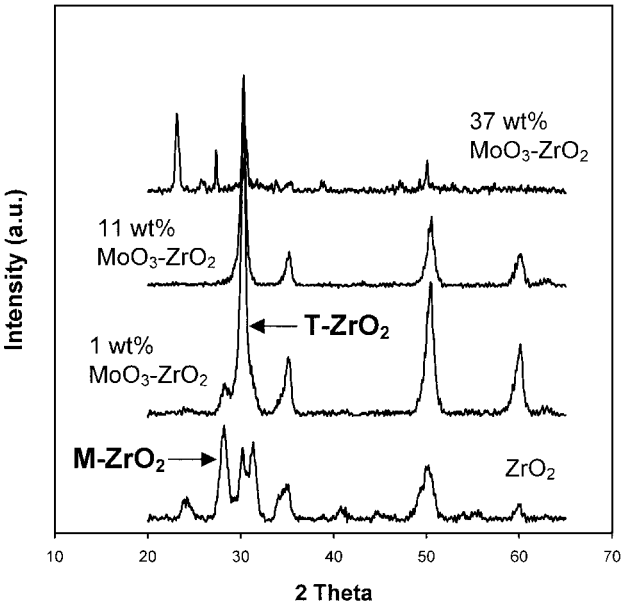

FIG. 4. XRD patterns of MoO_3–ZrO_2 catalysts with different MoO_3 concentrations treated in air at 773 K.

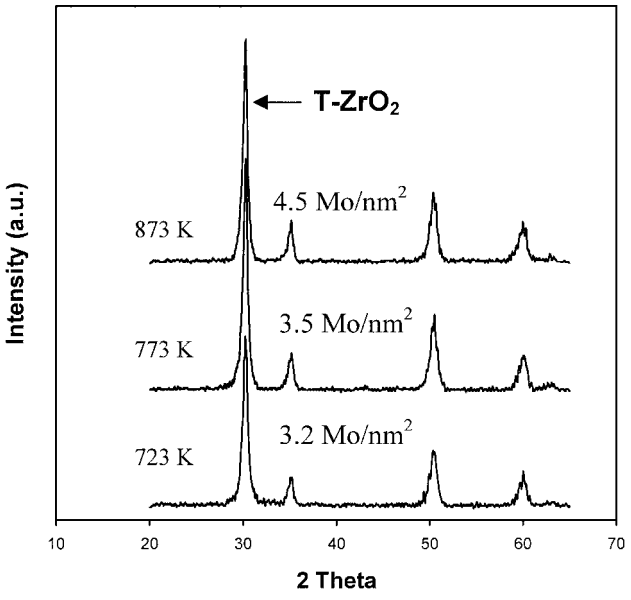

FIG. 5. XRD patterns of 11 wt% MoO_3–ZrO_2 catalysts treated in air at different temperatures.

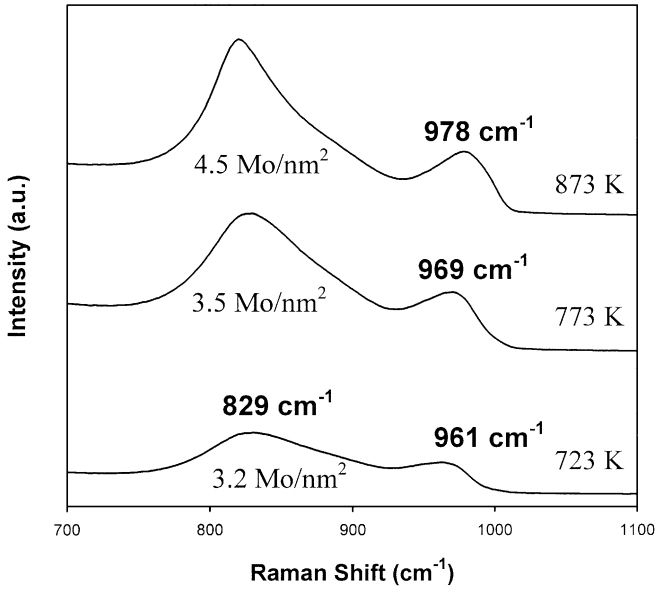

FIG. 7. Raman spectra of 11 wt% MoO_3–ZrO_2 catalysts treated in air at different temperatures.

reported in earlier studies (19, 22, 23), the Mo=O band shifts from 920 to 980 cm^{-1} with increasing Mo surface density. At high Mo surface densities (>10 Mo/nm^2), the Raman spectrum (Fig. 8) depends strongly on the treatment temperature. Bands at 748, 945, and 1000 cm^{-1}, assigned to $ZrMo_2O_8$ (19, 21), were detected in all samples treated at 873 K, but a treatment at 723 K led only to the appearance of bands at 819 and 995 cm^{-1}, corresponding to bulk MoO_3 (19, 21). The Raman spectra for samples with intermediate Mo surface densities (5–10 Mo/nm^2) (Fig. 9) were also influenced by the treatment temperature. After treatment at 873 K, bands were detected at 748, 945, and 1000 cm^{-1} corresponding to $ZrMo_2O_8$; a band at 819 cm^{-1}, assigned to bulk MoO_3, was also observed. Another band for bulk MoO_3 (at 995 cm^{-1}) was not clearly seen because it overlapped with the band at 1000 cm^{-1} for $ZrMo_2O_8$. MoO_x–ZrO_2 samples treated at 723 or 773 K showed a broad band at about 910 cm^{-1}, with a shoulder at about 942 cm^{-1}. Samples

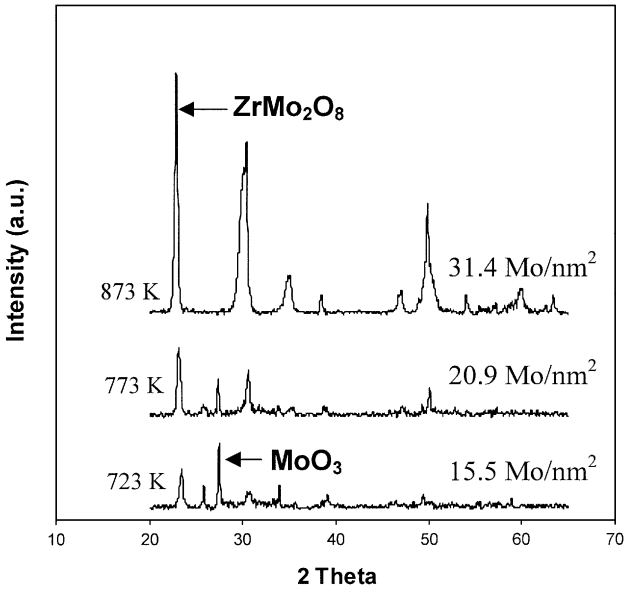

FIG. 6. XRD patterns of 37 wt% MoO_3–ZrO_2 catalysts treated in air at different temperatures.

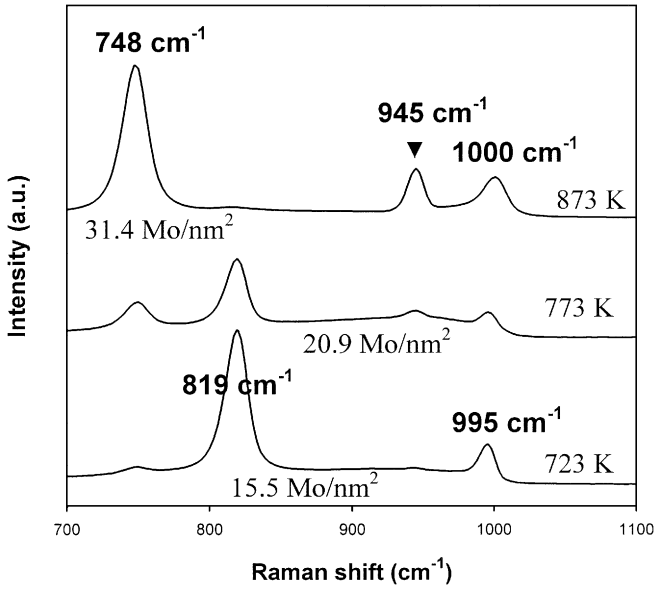

FIG. 8. Raman spectra of 37 wt% MoO_3–ZrO_2 catalysts treated in air at different temperatures.

of 5.8 wt% MoO_x/ZrO_2 prepared using ADM or AHM as precursors did not show detectable differences in their Raman spectra.

UV–visible absorption spectra reflect the electronic structure of valence bands in solids, but the broad nature of most charge trnasfer features prevalent in the spectra of metal oxides makes it difficult to define the position of these bands from the energy at maximum absorption. Absorption edge energies provide a more convenient description of the electronic properties of solids. The absorption edge in all UV–visible spectra was determined using Tauc's law for indirect and amorphous semiconductors using previously reported procedures (24). In this method, the absorption edge is defined as the intercept with the abscissa of the straight line describing the near-edge region for spectra plotted as $[F(R_\infty)h\nu]^{1/2}$, where $F(R_\infty)$ is the Kubelka–Munk function (25) and $h\nu$ is the energy of the incident photon. The position of the absorption edge for low-energy charge transfer transitions is shown to correlate with the domain size of oxides and other semiconductor and insulator materials (26–34). The absorption edge energy decreases with increasing domain size. This relationship was recently used to characterize the size of MoO_x (33), WO_x (26), and VO_x (14, 15) domains in catalytic solids.

Diffuse reflectance UV–visible spectra of MoO_x–ZrO_2 samples were measured and the absorption edge energies were calculated as described in the previous paragraph. The data are shown in Fig. 10 as a function of Mo surface density. Samples with very low Mo surface density (~0.4 Mo/nm^2) show edge energies (~3.46 eV) much lower than that of ammonium dimolybdate (3.80 eV). The absorption edge energy decreased initially with increasing Mo surface density, but then remained constant for Mo surface densities above 4 Mo/nm^2. The absorption edge energies (3.30 eV) for the latter samples were similar to those measured for bulk MoO_3 crystallites (3.29 eV).

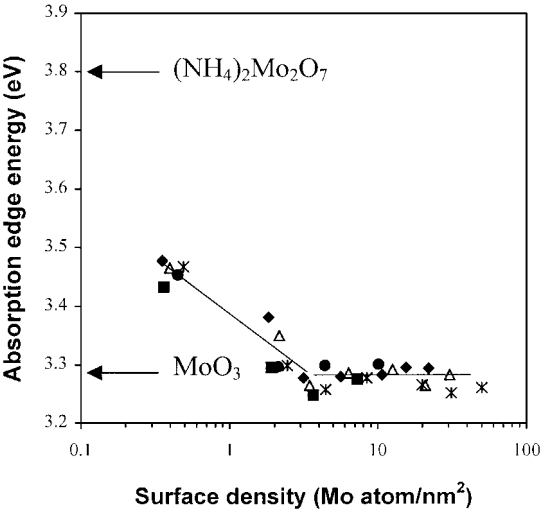

FIG. 10. Dependence of the UV–vis absorption edge energies on the Mo surface densities of MoO_x–ZrO_2 catalysts prepared using ADM as the precursor (pretreated in air at 723 K (◆), 773 K (△), and 873 K (∗)), and using AHM as the precursor (pretreated in air at 773 K (■) and 873 K (●)).

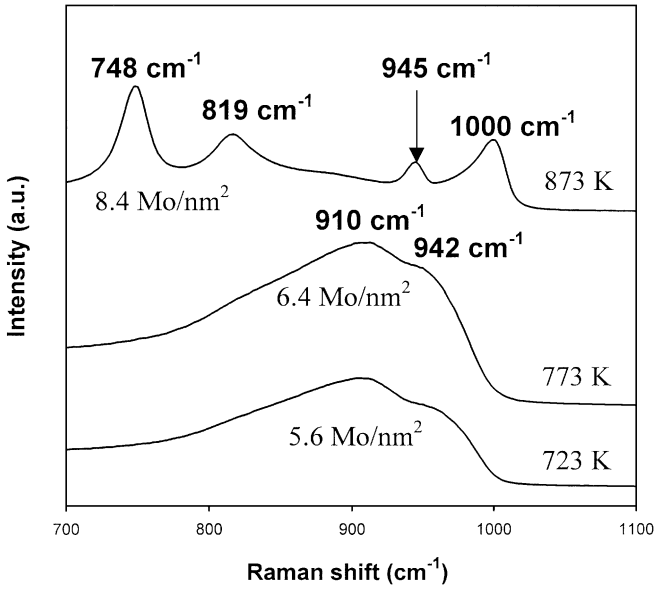

FIG. 9. Raman spectra of 20.7 wt% MoO_3–ZrO_2 catalysts treated in air at different temperatures.

Raman and XRD data showed that zirconia-supported molybdena samples can be grouped into two classes, based on the structure of the MoO_x species: (1) $ZrMo_2O_8/ZrO_2$ samples, which consist mainly of $ZrMo_2O_8$ supported on ZrO_2 and include all samples treated in air at 873 K with Mo surface densities higher than 5 Mo/nm^2, and (2) MoO_x/ZrO_2 samples, which consist of MoO_x species supported on ZrO_2 and include all samples treated in air at 723 and 773 K during synthesis as well as samples treated at 873 K but with Mo surface densities below 5 Mo/nm^2.

The catalytic properties of all MoO_x–ZrO_2 samples are reported in Figs. 11–13. Figure 11 shows the effect of bed residence time on C_3H_8 conversion and on C_3H_6, CO, and CO_2 selectivities for 11 wt% MoO_3/ZrO_2 treated in air at 773 K ($n_s = 3.5$ Mo/nm^2). The C_3H_6 selectivity decreased and the CO and CO_2 selectivities increased with increasing bed residence time, suggesting that C_3H_6 underwent secondary combustion reactions to form CO_x.

Initial propane conversion rates (normalized by the number of Mo atoms) are reported in Fig. 12 as a function of Mo surface density. They are referred to as turnover rates, even though not all MoO_x species are likely to be exposed at the surface of all samples. On MoO_x/ZrO_2 samples, turnover rates for propane conversion decreased monotonically with increasing Mo surface density. These turnover rates depended only on Mo surface density but not on the temperature of the air treatment or on the precursor used to prepare the catalysts. On $ZrMo_2O_8/ZrO_2$, the turnover

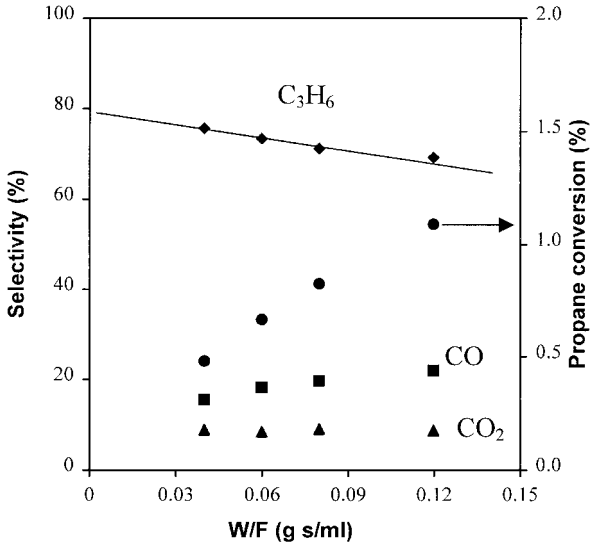

FIG. 11. Propane conversion and products selectivities for propane ODH on 11 wt% MoO_3–ZrO_2 catalysts calcined at 773 K.

rates also decreased with increasing Mo surface density. At the same Mo surface density, however, the reaction rates on $ZrMo_2O_8/ZrO_2$ samples were higher than those on MoO_x/ZrO_2 samples.

On MoO_x/ZrO_2 samples with Mo surface densities below 10 Mo/nm^2, the initial C_3H_6 selectivity (extrapolated to zero residence time) increased with increasing Mo surface density (Fig. 13). Above 10 Mo/nm^2, the initial C_3H_6 selectivity was about 93%, and it did not depend on Mo surface density. By contrast, the initial propene selectivity for $ZrMo_2O_8/ZrO_2$ remained constant (~80%) at all Mo surface densities.

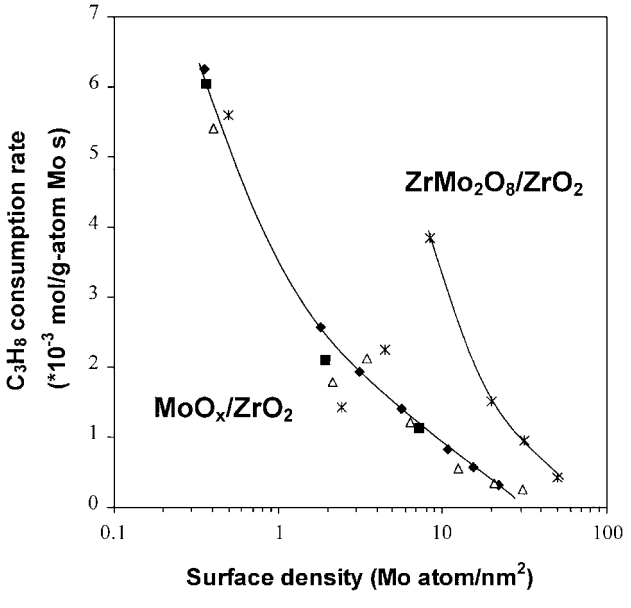

FIG. 12. Dependence of the propane consumption rates on the Mo surface densities of MoO_x–ZrO_2 catalysts prepared using ADM as the precursor (pretreated in air at 723 K (◆), 773 K (△), and 873 K (∗)), and using AHM as the precursor (pretreated in air at 773 K (■)).

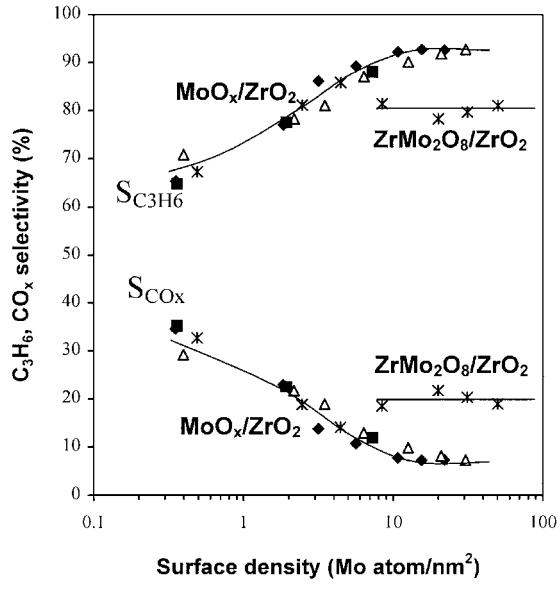

FIG. 13. Dependence of the propene and CO_x selectivities on the Mo surface densities of MoO_x–ZrO_2 catalysts prepared using ADM as the precursor (pretreated in air at 723 K (◆), 773 K (△), and 873 K (∗)), and using AHM as the precursor (pretreated in air at 773 K (■)).

DISCUSSION

The initial dispersion of MoO_x on the surface of zirconia influences both the surface area and the structure of the support. These effects are evident from the BET surface areas and the XRD data shown in Figs. 1–6. At MoO_3 loadings below 20 wt%, MoO_x species inhibit sintering of ZrO_2 and its transformation from the tetragonal to the monoclinic phase. These results are similar to those reported previously for VO_x/ZrO_2 (14) and WO_x/ZrO_2 (35).

The structure of dispersed molybdena species depends on the Mo surface density and, in some cases, also on the temperature of treatment in air. For samples with surface densities below 5 Mo/nm^2, Raman spectroscopy showed that MoO_x species are present exclusively as two-dimensional polymolybdate species. The absence of XRD peaks of Mo-containing species in these samples confirms the absence of large MoO_3 or $ZrMo_2O_8$ crystallites. The observed monotonic increase in the vibrational frequency of the Mo=O bond and the decrease in the UV–vis absorption edge energy are consistent with the growth of polymolybdate domains as the Mo surface density increases (23, 33). These conclusions are in agreement with those reported earlier by others (17–19).

For Mo surface densities above 10 Mo/nm^2, the structure of the dispersed MoO_x species depends strongly on the

treatment temperature. When samples were treated in air at 723 or 773 K, XRD and Raman spectroscopy detected bulk MoO_3 crystallites. The UV–visible absorption edge energies in such samples (3.30 eV) were almost identical to those in bulk MoO_3 (3.29 eV). Higher treatment temperatures (873 K) led to the disappearance of MoO_3 and to the detection of $ZrMo_2O_8$ in the XRD pattern and in the Raman spectrum. $ZrMo_2O_8$ was not formed in samples with Mo surface densities below 5 Mo/nm^2, even when treated at 873 K. This suggests that the formation of $ZrMo_2O_8$ requires MoO_3 crystallites as a precursor, in agreement with earlier observation of Miyata *et al.* (36).

For Mo surface densities between 5 and 10 Mo/nm^2, the catalyst structure depended on the treatment temperature as well as on the Mo surface density. Raman spectroscopy showed no evidence for either MoO_3 or $ZrMo_2O_8$ when oxidation occurred below 773 K; only polymolybdate species independent of the temperature of the air treatment were observed. Since the anticipated Mo surface density for monolayer coverage of ZrO_2 corresponds to 5 Mo/nm^2 (17–19), three-dimensional polymolybdate structures should be formed at higher Mo surface densities. While the UV–visable absorption edge energy for MoO_x/ZrO_2 samples with Mo surface densities above 5 Mo/nm^2 oxidized at below 773 K is identical to that for MoO_3, the absence of MoO_3 features in the Raman spectra of such samples suggests that the oxidation temperatures below 773 K are not high enough to transform the three-dimensional polymolybdate structures into MoO_3 crystallites. Crystallites of MoO_3 and $ZrMo_2O_8$ were both detected by Raman spectroscopy and XRD when the treatment temperature was raised to 873 K, suggesting that both MoO_3 and $ZrMo_2O_8$ were formed at high temperatures.

The data in Figs. 12 and 13 show that propane conversion rates and product selectivities changed markedly when dispersed MoO_x species react with ZrO_2 to form $ZrMo_2O_8$. Figure 12 shows that turnover rates for propane conversion decreased monotonically with increasing Mo surface density, but that for a given value of the apparent Mo surface density, turnover rates were higher on samples containing $ZrMo_2O_8$ than on those containing predominantly MoO_3 and polymolybdates. The decrease in turnover rates with increasing Mo surface density for samples with Mo surface densities lower than 5 Mo/nm^2 is accompanied by an increase in the vibrational frequency of Mo=O Raman bands (shown in Fig. 14), which reflects an increase in the strength of the Mo=O bond and a decrease in the ODH rectivity. Since monolayer polymolybdate coverage on ZrO_2 occurs at a Mo surface density of about 5 Mo/nm^2 (17–19), the decrease in the apparent turnover rate with increasing surface density is unlikely to arise from a decrease in the availability of Mo–O species at the catalyst surface when the Mo surface density is lower than 5 Mo/nm^2. What is suggested instead is that the catalyst activity decreases as the two-dimensional

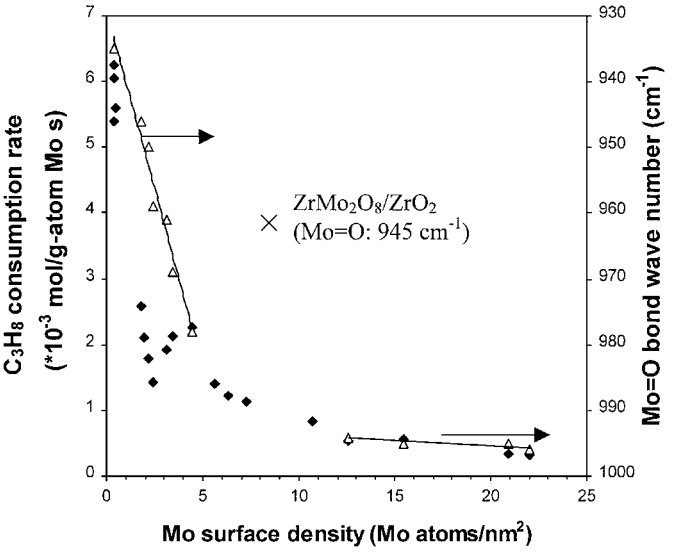

FIG. 14. Dependence of the propane conversion rate (◆) and Mo=O stretching frequency (△) on the Mo surface densities for MoO_x/ZrO_2 samples. The (×) symbol represents the propane conversion rate on a $ZrMo_2O_8/ZrO_2$ catalyst with a Mo surface density of 8.4 Mo/nm^2.

polymolybdate domains grow in size with increasing surface density. Since the rate-determining step in ODH involves activation of the C–H bond in C_3H_8 using lattice oxygen atoms (16), it is reasonable to expect the ODH rate to depend on the strength of the Mo=O bond. For Mo surface densities above 5 Mo/nm^2, the observed decrease in the turnover rate is ascribed to the lower propane accessibility due to the formation of three-dimensional polymolybdate structures or small crystallite MoO_3.

MoO_x species present in $ZrMo_2O_8/ZrO_2$ give higher apparent turnover rates than three-dimensional polymolybdate species in MoO_x/ZrO_2 of similar Mo surface densities (Fig. 12). The higher turnover rates on $ZrMo_2O_8$ reflect the fact that the Mo=O bonds in this material are weaker than those in three-dimensional polymolybdate species. Structural analysis of $ZrMo_2O_8$ shows that the Mo^{6+} cations are located in tetrahedral sites (37). Of the four oxygens surrounding each Mo^{6+} cation, one is bonded only to Mo while the other three are shared by a Zr^{4+} cation and a Mo^{6+} cation. The Mo–O bond length for the oxygen atom associated only with Mo^{6+} is 1.690 Å, and the other three Mo–O bonds have an average length of 1.764 Å. Based on a correlation reported between the Mo–O bond length and vibrational frequency (38), the shorter Mo–O bond in $ZrMo_2O_8$ is assigned to Mo=O vibrations. The frequency at 945 cm^{-1} is considerably lower than that for Mo=O bonds in either MoO_3 (995 cm^{-1}) or in a polymolybdate monolayer (985 cm^{-1}) (see Fig. 14). Following this logic, the apparent turnover rate of $ZrMo_2O_8$ might be expected to be equivalent to that of polymolybdate species exhibiting a similar Mo=O bond vibrational frequency (Mo surface

density is ~2 Mo/nm^2). Figure 14 shows that the rate predicted by this means is about ~20% higher than that measured for $ZrMo_2O_8$, which may be ascribed to the decrease in Mo=O availability as a consequence of the three-dimensional character of $ZrMo_2O_8$. The decrease in the apparent turnover rate (normalized to the total Mo content) with increasing Mo surface density also reflects the expected decrease in the dispersion of the supported $ZrMo_2O_8$ crystallites as the Mo content increased or the total surface area decreased.

The data in Fig. 13 show that the selectivities to C_3H_6 and CO_x also depend on whether $ZrMo_2O_8$ or dispersed MoO_x species are present. On samples containing predominantly polymolybdate or MoO_3 species, initial C_3H_6 selectivities increased with increasing surface density and reached a constant value (93%) above 10 Mo/nm^2. On $ZrMo_2O_8$ samples, the propene selectivity is lower than this value (~80%), but independent of Mo surface density (10–50 Mo/nm^2). The gradual increase in C_3H_6 selectivity with increasing Mo surface density suggests that high selectivity may require complete coverage of the ZrO_2 surface by a mixture of molybdate oligomers; i.e., the exposure of the Zr–O–Mo bond is unfavorable for selective oxidation. Similar conclusions have also been obtained with VO_x/ZrO_2 (14). The gradual increase in C_3H_6 selectivity with increasing Mo surface density may also be related to the increase in the strength of Mo=O bonds in MoO_x species with increasing domain size—stronger Mo=O bonds being associated with higher selectivity, albeit lower activity. Consistent with these proposals, $ZrMo_2O_8$ catalysts show C_3H_6 selectivities lower than that of MoO_3. The absence of surface density effects on the initial C_3H_6 selectivity of $ZrMo_2O_8$-containing samples confirms the proposal that $ZrMo_2O_8$ domains increase in size with increasing Mo surface density without significant changes in their local structure or surface properties.

The observed effects of residence time on product selectivity (Fig. 11) are consistent with C_3H_8–O_2 reactions occurring via parallel and sequential steps, as shown below.

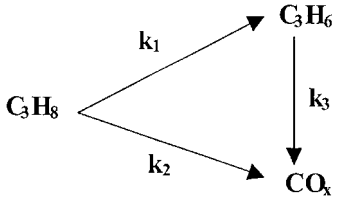

Pseudo-first-order rate coefficients for primary dehydrogenation (k_1) and combustion (k_2) pathways and for secondary combustion of propene (k_3) can be obtained from the measured effects of reactor residence time data on product concentrations (1–3). The assumption that all steps are proportional to the respective hydrocarbon concentration was confirmed experimentally for MoO_x–ZrO_2 catalysts.

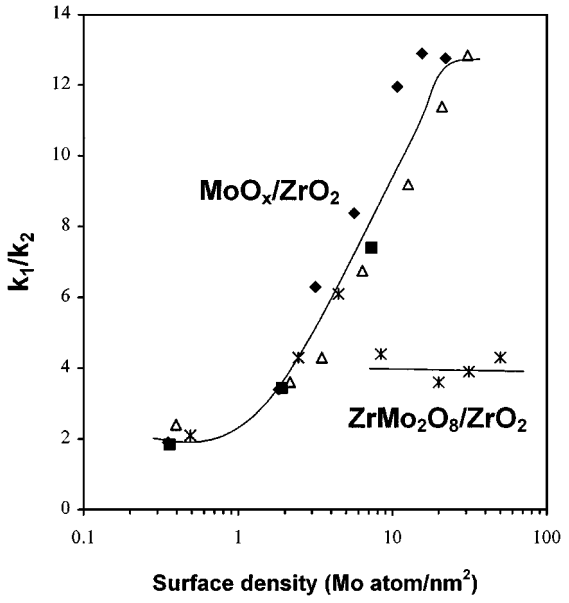

FIG. 15. Dependence of the k_1/k_2 ratios on the Mo surface densities for MoO_x–ZrO_2 catalysts prepared using ADM as the precursor (pretreated in air at 723 K (◆), 773 K (△), and 873 K (∗)), and using AHM as the precursor (pretreated in air at 773 K (■)).

Figures 15 and 16 show the effects of Mo surface density on k_1/k_2 and k_3/k_1. The dependence of k_1/k_2 on Mo surface density is very similar to that observed for the initial C_3H_6 selectivity (Fig. 13), and it reflects the relative rates of ODH

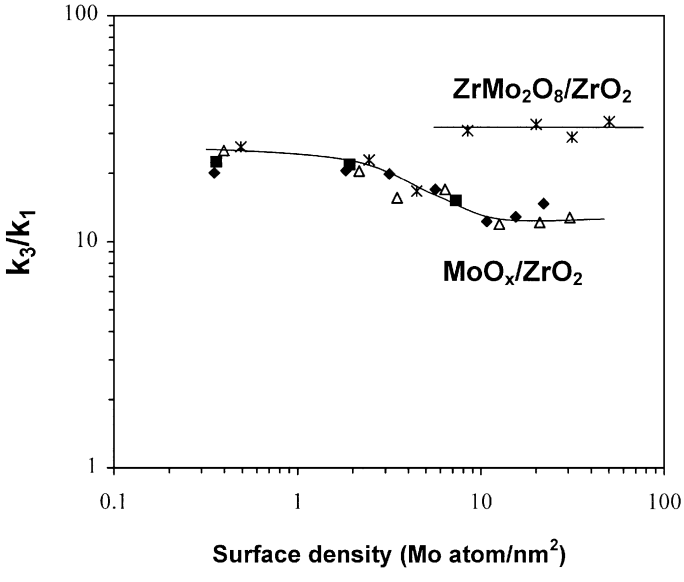

FIG. 16. Dependence of the k_3/k_1 ratios on the Mo surface densities of MoO_x–ZrO_2 catalysts prepared using ADM as the precursor (pretreated in air at 723 K (◆), 773 K (△), and 873 K (∗)), and using AHM as the precursor (pretreated in air at 773 K (■)).

and C_3H_8 combustion reactions. On $ZrMo_2O_8/ZrO_2$, k_1/k_2 remained constant at a value of about 4 for the Mo surface densities of 10–50 Mo/nm^2. On MoO_x/ZrO_2, however, k_1/k_2 increased with increasing Mo surface density and reached a maximum value of about 13 for surface densities above 10 Mo/nm^2. The k_1/k_2 ratios measured on samples treated at 773 K were a little bit lower than those for samples treated in air at 723 K for all Mo surface densities above 5 Mo/nm^2. This is attributed to the presence of small amounts of $ZrMo_2O_8$ (detected by Raman) in addition to the predominant MoO_x species. As shown in Fig. 15, the value of k_1/k_2 for $ZrMo_2O_8/ZrO_2$ is lower than that for MoO_3/ZrO_2.

On every sample examined, k_3/k_1 ratios were much greater than unity (Fig. 16), indicating that propene combustion occurs more rapidly than propane ODH. This is the main reason why propene selectivities decrease markedly as propane conversion increases. The range of k_3/k_1 values (10–40) on all catalysts is similar to that measured on VO_x/ZrO_2 catalysts at 603 K (14, 15). The k_3/k_1 ratio on $ZrMo_2O_8/ZrO_2$ is higher than that on MoO_x/ZrO_2 at similar Mo surface densities. On MoO_x/ZrO_2, k_3/k_1 decreased slightly with increasing Mo surface density and then remained constant for Mo surface densities above 10 Mo/nm^2. These results confirm the proposal that exposure of Mo–O–Zr bonds favors the combustion of propene.

CONCLUSIONS

The structure of MoO_x species dispersed on zirconia depends strongly on the Mo surface density and on the temperature of thermal treatment, but not on the composition of the precursors or pH of the impregnation solution. Two-dimensional polymolybdate MoO_x species are favored in samples with Mo surface densities lower than that calculated for a polymolybdate monolayer (5 Mo/nm^2). At surface densities above 5 Mo/nm^2, the structure of MoO_x species depends strongly on the temperature of the catalyst oxidation. Low temperatures (723 K) lead to the sintering of polymolybdate into MoO_3 crystallites, whereas high-temperature treatments (above 773 K) lead to the observation of $ZrMo_2O_8$ by reaction between MoO_3 and ZrO_2. Catalysts can be divided into two types based on molybdenum-containing species structures: MoO_x/ZrO_2, which mainly consists of MoO_x and ZrO_2, and $ZrMo_2O_8/ZrO_2$, which is mainly composed of $ZrMo_2O_8$ dispersed on ZrO_2.

Catalytic and spectroscopic data showed that MoO_x and $ZrMo_2O_8$ are active in propane oxidative dehydrogenation. On both $ZrMo_2O_8/ZrO_2$ and MoO_x/ZrO_2 catalysts, turnover rates (per total Mo atoms) decrease with increasing Mo surface density because of either the lower propane accessibility or lower Mo=O bond reactivity as MoO_x domains grow. Mo=O bonds are active for C–H bond activation. Weaker Mo=O bonds lead to higher catalytic activity because they are involved in rate-determining C–H bond activation steps requiring lattice given oxygen atoms. The exposure of Mo–O–Zr bonds is undesirable since they contribute to the combustion of C_3H_6 to CO_x.

ACKNOWLEDGMENTS

This work was supported by the Director, Office of Basic Energy Sciences, Chemical Science Division of the U.S. Department of Energy under Contract DE-AC03-76SF00098.

REFERENCES

1. Blasko, T., and López Nieto, J. M., *Appl. Catal. A* **157**, 117 (1997).
2. Kung, H. H., *Adv. Catal.* **40**, 1 (1994).
3. Albonetti, S., Cavani, F., and Trifiro, F., *Catal. Rev.-Sci. Eng.* **38**, 413 (1996).
4. Centi, G., and Triffiro F., *Appl. Catal. A* **143**, 3 (1996).
5. Mamedov, E. A., and Cortés-Corberan, V., *Appl. Catal. A* **127**, 1 (1995).
6. Meunier, F. C., Yasmeen, A., and Ross, J. R. H., *Catal. Today* **37**, 33 (1997).
7. Cadus, L. E., Gomez, M. F., and Abello, M. C., *Catal. Lett.* **43**, 229 (1997).
8. Yoon, Y. S., Fujikawa, N., Ueda, W., Moro-oka, Y., and Lee, K. W., *Catal. Today* **24**, 327 (1995).
9. Yoon, Y. S., Ueda, W., and Moro-oka, Y., *Top. Catal.* **3**, 256 (1996).
10. Lee, K. H., Yoon, Y. S., Ueda, W., and Moro-oka, Y., *Catal. Lett.* **46**, 267 (1997).
11. Mercera, P. D. L., van Ommen, J. G., Desburg, E. B. M., Burggraaf, A. J., and Ross, J. R. H., *Appl. Catal.* **57**, 127 (1990).
12. Mercera, P. D. L., van Ommen, J. G., Desburg, E. B. M., Burggraaf, A. J., and Ross, J. R. H., *Appl. Catal.* **71**, 363 (1991).
13. Iglesia, E., Barton, D. G., Soled, S. L., Miseo, S., Baumgartner, J. E., Gates, W. E., Fuentes, G. A., and Meitzner, G. D., *Stud. Surf. Sci. Catal.* **101**, 533 (1996).
14. Khodakov, A., Yang, J., Su, S., Iglesia, E., and Bell, A. T., *J. Catal.* **177**, 343 (1998).
15. Khodakov, A., Olthof, B., Bell, A. T., and Iglesia, E., *J. Catal.* **181**, 205 (1999).
16. Chen, K., Khodakov, A., Yang, J., Bell, A. T., and Iglesia, E., *J. Catal.* **186**, 325 (1999).
17. Prinetto, F., Cerrato, G., Ghiotti, G., Chiorino, A., Campa, M. C., Gazzoli, D., and Indovina, V., *J. Phys. Chem.* **99**, 5556 (1995).
18. Afanasiev, P., *Mater. Chem. Phys.* **47**, 231 (1997).
19. Liu, Z., and Chen, Y., *J. Catal.* **177**, 314 (1998).
20. Indorina, V., *Catal. Today* **41**, 95 (1998).
21. Mestl, G., and Srinivasan, T. K. K., *Catal. Rev.-Sci. Eng.* **40**, 451 (1998).
22. Dufresne, P., Payen, E., Grimblot, J., and Bonnelle, J. P., *J. Phys. Chem.* **85**, 2344 (1981).
23. Ohno, T., Miyatu, H., and Kubokawa, Y., *J. Chem. Soc., Faraday Trans.* **83**, 1761 (1987).
24. Tauc, J., *in* "Amorphous and Liquid Semiconductors", (J. Tauc, Ed.). Plenum, London, 1974.
25. Delgass, W. N., "Spectroscopy in Heterogeneous Catalysis." Academic Press, New York, 1979.
26. Barton, D. G., Shtein, M., Wilon, R. D., Soled, S. L., and Iglesia, E., *J. Phys. Chem. B* **103**, 630 (1999).
27. Cherstnoy, N., Hull, R., and Brus, L. E., *J. Chem. Phys.* **85**, 2237 (1986).

28. Alivisatos, A. P., *Science* **271**, 933 (1996).
29. Service, R. F., *Science* **271**, 920 (1996).
30. Hoener, C. F., Allan, K. A., Bard, A. J., Campion, A., Fox, M. A., Mallouk, T. E., Webber, S. E., and White, J. M., *J. Phys. Chem.* **96**, 3812 (1992).
31. Liu, Z., and Davis, R. J., *J. Phys. Chem.* **90**, 2555 (1986).
32. Wang, Y., Mahler, S. W., and Kasowski, R., *J. Chem. Phys.* **87**, 7315 (1987).
33. Weber, R. S., *J. Catal.* **151**, 470 (1995).
34. Fournier, M., Louis, C., Che, M., Chaquin, P., and Masure, P., *J. Catal.* **119**, 400 (1989).
35. Barton, D. G., Soled, S. L., Meitzner, G. D., Fuentes, G. A., and Iglesia, E., *J. Catal.* **181**, 57 (1999).
36. Miyata, H., Tokauda, S., Ono, T., Ohno, T., and Hatayama, F., *J. Chem. Soc., Faraday Trans.* **86**, 2291 (1990).
37. Auray, B. M., Quarton, M., and Tarte, P., *Acta. Crystallogr.* **C42**, 257 (1986).
38. Hardcastle, F. D., and Wachs, I. E., *J. Phys. Chem.* **21**, 683 (1990).